UNIWERSYTET TECHNOLOGICZNO-PRZYRODNICZY
IM. JANA I JĘDRZEJA ŚNIADECKICH
W BYDGOSZCZY

WYDZIAŁ TELEKOMUNIKACJI
I ELEKTROTECHNIKI

ZESZYTY NAUKOWE NR 254

ELEKTROTECHNIKA
14

BYDGOSZCZ – 2009

UNIWERSYTET TECHNOLOGICZNO-PRZYRODNICZY
IM. JANA I JĘDRZEJA ŚNIADECKICH
W BYDGOSZCZY

ZESZYTY NAUKOWE NR 254

ELEKTROTECHNIKA
14

BYDGOSZCZ – 2009

REDAKTOR NACZELNY
prof. dr hab. inż. Janusz Prusiński

REDAKTOR DZIAŁOWY
dr inż. Sławomir Cieślik

OPRACOWANIE TECHNICZNE
mgr Patrycja Fereni-Morzyńska

ISSN 0209-0570

Wydawnictwa Uczelniane Uniwersytetu Technologiczno-Przyrodniczego
ul. Ks. A. Kordeckiego 20, 85-225 Bydgoszcz, tel. (052) 3749482, 3749426
e-mail: wydawucz@utp.edu.pl http://www.utp.edu.pl/~wyd

Wyd. I. Nakład 80 egz. Ark. aut. 2.0. Ark. druk. 2.25.
Zakład Małej Poligrafii UTP Bydgoszcz, ul. Ks. A. Kordeckiego 20

Contents

UNIWERSYTET TECHNOLOGICZNO-PRZYRODNICZY
IM. JANA I JĘDRZEJA ŚNIADECKICH W BYDGOSZCZY
ZESZYTY NAUKOWE NR 254
ELEKTROTECHNIKA 14 (2009), 5-16

ENERGY EFFICIENT, MULTICRITERION INTELLIGENT CONTROL SYSTEM OF THE ELECTRICAL REGIMES OF ARC STEEL-MELTING FURNACE

O.Yu. Lozinskyy, A.O. Lozinskyy, R.Ya. Paranchuk, Ya.S. Paranchuk

Lvivska Politekhnika National University –
Power Engineering And Control Systems Institute
79013, Bandery str., 13, Lviv, Ukraine
lozynsky@polynet.lviv.ua, rparanchuk@gmx.net

Summary: Hierarchical structure of a system of adaptive multicriterion control of a three-phase arc steel furnace electrical modes is proposed. Models of optimal control vector synthesis were developed. Adaptation of control is performed depending on technological stages, which are identified by neural network.

Keywords: arc steel-melting furnace, neural network, control system

1. INTRODUCTION

Contemporary state of metal production industry is characterized by continuous growth of part of steels melted in three-phase electric arc furnaces (EAF). These steel-melting installments are characterized by large steady-state power of furnace transformer up to 1 MV·A/ton. They are characterized by highly dynamic, nonlinear and non-symmetrical load. Also, arc furnaces functioning is accompanied by technological short circuits and unstable, discontinuous burning of arcs and it can lead to oscillations of arc power, which are commensurable with furnace transformer power. Moreover, furnace functioning leads to oscillations, nonlinear shape distortions and non-symmetry in power system voltage. Four important problems arose during exploiting of arc furnaces:

1. Ensuring maximum arc power during melting of solid charge.
2. Qualitative stabilization of arc power.
3. Minimization of specific power losses.
4. Limiting nonlinear and varying load impact on power system.

Mentioned problems significantly increased in high-power and high-impedance furnaces with arc voltages of 1000-1500 Volts and specific power of 1 MV·A/ton. In general, these problems are contradictory and can be solved only with toleration of some compromises.

Solution of mentioned task requires adequate improvements of melting technology, development of new efficient melting systems and also creation of hierarchical intelligent systems of adaptive optimal control and high-speed multi-circuit systems for electric regime coordinates control. Moreover, high arc current amplitude oscillations

lead to vibrations and significant electrodynamic forces in the windings of electrical power equipment, which decreases its functional reliability and life time. This is mainly caused by the low dynamic accuracy of controlling the electrical-regime parameters because of the significant sluggishness of existing electromechanical (electrohydraulic) electrode-position control systems.

Nowadays, the part of electrical steels in the total steel output is increasing, the power of an electric furnaces is increasing, and, as the result, melting process is intensified [1,2]. Therefore, it is important to improve the electrical and technical efficiency of arc furnaces and the electromagnetic compatibility of the electrical-regime parameters with the power system parameters.

As for the technical and economic assessment, the optimum control of electric melting is known to be two to three times as efficient as the solutions intended for stabilizing electrical regime parameters [3]. Nevertheless, these problems should be solved jointly, since the qualitative stabilization of electrical-regime parameters at the level of synthesized optimum values additionally increases the control efficiency. Therefore, the main methods of increasing the electrical and technical efficiency of melting in arc steel furnaces are represented by developing control circuits and synthesis of optimal control methods. They are intended for minimization of dispersion of the electrical regime coordinates and stabilizing them at the level of synthesized optimum values.

2. ANALYSIS OF KNOWN SOLUTIONS

The functions of most existing EAF electrical-regime control systems (e.g., ARDG, ARDMT, RMM, and STU arc-power controllers) are mainly limited to the maintenance of a specified phase impedance, arc voltage, or arc current depending on the voltage of the secondary winding of a furnace transformer (FT). As noted above, high oscillations in the electrical-regime parameters, which are caused by the low dynamic accuracy of their control and the limited functional optimization abilities of the above mentioned controllers given do not allow one to substantially increase the efficiency of the EAF heat-regime control.

To improve the electromagnetic compatibility of the arc-furnace electrical operating conditions with the power system conditions, static filter-compensating devices are widely used in metallurgy, which should compensate for the negative effects of a furnace on the power system. Of course, such solutions are often required. But we believe that metallurgists should mainly obtain automatic and algorithmic solutions intended for the suppression of the causes of disturbances in their origin (in the power circuit of an arc furnace), i.e., solutions intended to anticipate the appearance of negative actions on the technical and economic indices of the furnace and the electromagnetic compatibility of the furnace electrical operating conditions with the power system conditions.

The authors of [4] give an example of the realization of this direction in increasing the efficiency of controlling the EAF electrical conditions; they describe an EAF power system that includes a saturating reactor. In furnaces with such a power system and high impedance, metallurgists can increase the EAF transformer power via increasing the secondary voltage and can run a heat using long arcs. These solutions can decrease the arc-current dispersion, increase the arc stability, and decrease the short-circuit probability, all other things being equal.

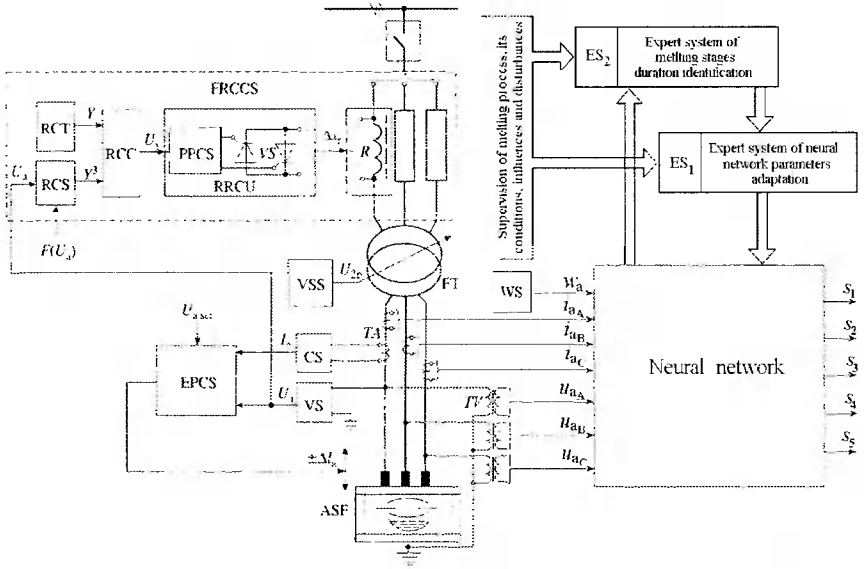

Fig. 1. Functional schematic diagram of the power and electrical-regime control system for an EAF with neural-network-based melting stages recognition: FRCCS is the regime coordinate control subsystem; RCS and RCT, regime coordinate set-point device and transducer, respectively; RCC, regime coordinate controller; RRCU, reactor-resistance control unit; PPCS, pulse-phase control system; *VS*, thyristor unit; *R*, reactor; EPCS, electrode-position control subsystem; CS and VS, current and phase-voltage sensors, respectively; FT, furnace transformer; and VSS, transformer voltage step switch; ES_1 and ES_2, expert systems.

However, when the method of controlling the reactor resistance proposed in [4] is used, a single type of artificial external characteristics (AECs) in a furnace, i.e., arc current-voltage characteristics ($I_a(U_a)$), is only realized. This type is represented by characteristics such that the arc currents are stabilized in the range of low and medium arc voltages (short and long arcs). The arc current is a controlled parameter in such furnace AECs at a given voltage step of a furnace transformer, and the arc current is specified by the bias current of the saturating reactor. This scheme restricts the functional possibilities of the system in the realization of various optimum strategies of controlling EAF regimes using partial criteria or generalized target functionals, which are formed with allowance for current heat conditions and current requirements for the technical and economic indices of an arc furnace. Moreover, the realization of this control requires a significant preset power of the saturating reactor, and the shape of the electric current during control is close to a rectangular shape. The fabrication of such a saturating reactor requires high-quality magnetic materials with oriented crystals.

3. TWO-CIRCUIT HIGH-SPEED CONTROL SYSTEM

To realize these directions in increasing the control efficiency, we propose a two-circuit coordinate-parameter hierarchical automatic control system (CS) for an EAF electrical regime with automatic neural network based identification of technologic stages (Fig. 1).

In this two-circuit system, regime coordinates, i.e., electrical regime coordinates such as the arc current, arc power, and furnace reactive power (which change according to their specific laws), are rapidly controlled and stabilized at a given level using the thyristor-assisted control of the resistance of a reactor located in the primary winding circuit of the furnace transformer. Conventional single-phase current-limiting nonsaturating reactors, which do not require special magnetic materials for their magnetic system, are used as the reactor in each furnace-power phase.

This CS of melting modes consists of two subsystems (control circuits), namely, an electrode position control subsystem (EPCS) and a furnace-regime coordinate-control subsystem (FRCCS). These systems operate simultaneously and independently and have isolated phases.

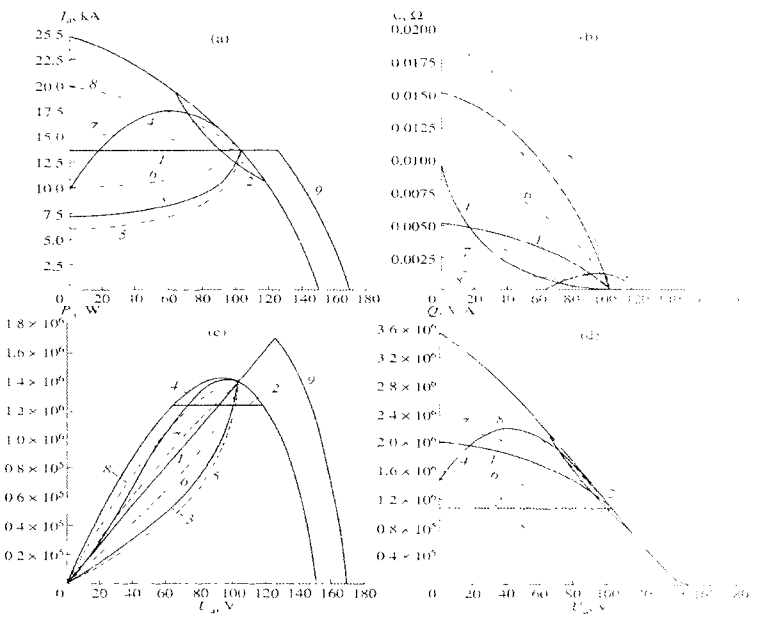

Fig. 2. Electrical characteristics of a DSP-6 arc steelmaking furnace with a two-circuit electrical-regime control system (the numerals on the curves are explained in the text).

The first subsystem is an ordinary electrode-position control system with an electromechanical or hydraulic actuator, which controls the change in the arc length $\pm\Delta l_a$. The control of the arc length is indirectly realized as a function of the current values of arc current I_a and voltage U_a, and the signals proportional to these values are generated at the output of an arc current or voltage sensor, respectively. An arc-voltage setting signal $U_{a\,set}$, which is proportional to I_a, is the master control of this subsystem. If necessary, transformer voltage steps can be switched using VSS devices.

The FRCCS subsystem is intended for controlling a furnace-regime coordinate (electrical-regime parameter), such as the arc current, arc power, or furnace-reactive power.

A change in the reactor resistance Δx_r is the master control of this subsystem. In each phase, this change is controlled smoothly and continuously via shunting the reactor by a VS thyristor unit in a certain controlled segment of a powering voltage half-cycle. The segment time is determined by the phase of the output signal of a pulse-

phase control system (PPCS), and this signal, in turn, forms as an autocorrelation function of the output signal U_y of a proportional-integral furnace regime coordinate controller (RCC). The input of this controller receives Y^3 signals from a set-point device and Y signals from the sensor of a certain controlled furnace-regime coordinate. In the general case, the setting signal Y^3 of this subsystem is a function of the arc voltage, which enters into the input of a furnace-regime coordinate set-point device (RCS). In particular, upon the stabilization of a regime coordinate, signal Y^3 is a constant, which determines the required level of regime-coordinate stabilization. In the general case, setting signal Y^3 is calculated in the RCS from a $Y^3 = F(U_a)$ relation, which is the setting action of this subsystem (this is especially effective for the realization of the adaptive multicriterion control of an EAF electrical-heat regime). Compared to the electromechanical EPCS subsystem, the speed of this subsystem is higher by an order of magnitude: its response time is 0.03-0.04 s. For the reactor resistance to be controlled with a thyristor, metallurgists developed solutions so that the distortion of the sinusoidal furnace-loading currents is minimal.

4. MELTING STAGES RECOGNTION SYSTEM

One of the prerequisites of guaranteed production of steels and alloys with desired physical and chemical properties and of high technological and economical efficiency during melting process is synthesis and implementation of two-circuit system control vector depending on technological melting stage. Therefore one of main problems is recognition of technological melting stages and moments of their changes.

Most efficient approach to technological stages recognition under conditions of insufficient information about technological process and its stochastic fluctuations is recognition based on neural networks principles. For implementation of such approach, three-layer neural-network- based expert system is included into control system. It is used for recognition of melting stages S_1, S_2, ..., S_5 (Fig.1). Input information of the neural network is vector of instantaneous values of arc voltages $u_{a.1}$, u_{aB}, u_{aC}, currents $i_{a.1}$, i_{aB}, i_{aC} and consumed on current stage active energy w_a [5,6]. Informative parameters of mentioned electrical mode coordinates time dependencies are averaged values on stationarity intervals of their canonical harmonics (they are calculated using FFT method). Also, power spectrums of voltages U_a and currents I_a in informative frequency range are taken into account. They are calculated using the fast wavelet transform technique. Dispersion, correlation coefficient and total harmonic distortions (THD) coefficients of currents and voltages are used too. Algorithm of operative calculation of mentioned parameters integral values is implemented using microprocessor device. Optimal parameters of three-layer neural network used for melting stages recognition were obtained, training and testing performed. Industrial testing of network was performed on arc furnace DSP-3. This neural network forms the first level of melting stages recognition hierarchical system.

On the second level there is expert system ES_1, which serves for adaptive optimization of neural network variable coefficients (coefficients of synaptic relations). This expert system is of production type, in other words is it based on "instructive knowledge" – in form of production rules "If ... Then ..." This expert system, basing on expert knowledge and operative input information, performs discrete parametric optimiza-

tion of neural network to parameters of furnace charge. It loads from database synthesized matrix of synaptic relations, which corresponds to current type, density and stowing of hard charge, changes transfer constant of active energy measuring channel proportionally to the weight and temperature of loaded charge. Knowledge base of expert system is assembled from formalized technical specialists' experience.

On the third, highest level of hierarchy expert system ES_2 is used, which processes expert knowledge from exact analysis of melting stages changes. If identification error is greater then certain threshold, ES_2 initializes procedure of learning (adjusting) to slowly varying conditions of melting process: current state of furnace cladding, power supply parameters, external temperature, etc.

Developed expert hierarchical neural-network-based system for melting stages recognition naturally combines advantages of neural networks and expert systems. Neural networks have capability of operative parametrical adaptation and expert systems make it possible to relatively simple identify moments of adaptation algorithms start.

This ensures small error of melting stage change moments identification. Error didn't exceed 5% during experiment melting in DSP-3 furnace.

5. ELECTRICAL CHARACTERISTICS OF A TWO-CIRCUIT CS

Fig. 2a shows the natural and artificial external characteristics of a DSP-6 arc furnace in the first step of the furnace transformer. Artificial external $I_a(U_a)$ characteristics *7*, *2*, and *3* are formed by the two-circuit coordinate-parameter control system upon the stabilization of the arc current, arc power, and furnace reactive power in the zone of short and medium arc lengths. Fig. 2b shows the corresponding reactor resistance $x_r(U_a)$ curves for characteristics *1*, *2*, and *3*. Fig. 2c and 2d show the artificial characteristics of the arc power ($P_a(U_a)$) and furnace reactive power ($Q(U_a)$) corresponding to characteristics *1*, *2*, and *3*. For the artificial furnace characteristics corresponding to characteristics *1* and *2*, we obtained the following $x_r(U_a)$ dependences for controlling the reactor resistance:

$$x_r^I(U_a) = \frac{\sqrt{U_{2p}^2 - U_a^2 - 2rU_a I_{as} - r^2 I_{as}^2}}{I_{as}} - x;$$

$$x_r^{I'}(U_a) = \frac{\sqrt{U_a^2 - (U_{2p}^2 - U_a^2 - 2rP_{as}) - r^2 P_{as}^2}}{P_{as}} - x;$$

where:

U_{2p} – secondary-phase voltage of the electric-furnace transformer,
r, x – active and reactive current-lead resistances, respectively,
I_{as}, P_{as} – levels of arc-current stabilization and arc-power stabilization, respectively.

The problem of coordinate stabilization during regime optimization is a partial problem. In the general case, the proposed two-circuit CS can realize other $I_a(U_a)$ AECs, e.g., those of type *4* (Fig. 2) or similar to the family of dashed curves *5*,*6*,*7* and *8*. For these and related AECs, we obtained models for the calculation of the corresponding reactor resistances $x_r^{I'}(U_a)$.

In the general case, we take into account a synthesized $x_r(U_a)$ dependence and calculate the artificial external characteristics of a furnace using the expression

$$I_a(U_a) = \frac{-U_a r + \sqrt{(rU_a)^2 + (r^2 + (x + x_r(U_a))^2)(U_{2p}^2 - U_a^2)}}{r^2 + (x + x_r(U_a))^2}. \quad (1)$$

In particular, AECs of types *1*,*3*,*5*,*6*,*7*, or *8* (Fig. 2) are calculated from (1) via multiplying a forming coefficient γ from the basic regulation law $x_r(U_a) = \gamma\, x_r^b\,(U_a)$. The basic regulation law is taken to be a $x_r(U_a)$ law corresponding to characteristics *1* or *3*. We assumed that the basic regulation law corresponds to characteristic *3*, i.e., $x_r(U_a) = x_r^Q(U_a) = x_r^b(U_a)$, where $\gamma = 1$. When substituting $x_r(U_a) = \gamma\, x_r^b\,(U_a)$ into (1) and changing the values of γ in the range from 0 to 1.25, we calculate the family of characteristics *8*, *7*, *1*, *6*, *3*, and *5* located between the natural external furnace characteristic ($\gamma = 0$) and AECs of type *5* ($\gamma = 1.25$).

When AECs are formed via adjusting the reactor resistance, the arc power $P_a(U_a)$ decreases with respect to the power for the natural characteristic ($x_r(U_a) = 0$). To compensate for this decrease and to increase (if necessary) the average arc power, it is sufficient to increase the secondary voltage of the furnace transformer (Fig. 2, characteristic 9) by 10-30%, which corresponds to modern trends in the intensification of the regimes of high-impedance long-arc furnaces [1,2].

In the general case, the control vector $\vec{x}\,(U_{2p},\ U_{a\text{-}set},\ \gamma_1, \gamma_2, \ldots)$ contains the secondary voltage of the furnace transformer U_{2p}; the arc-voltage setting $U_{a\text{-}set}$ of the electrode-position controller; and the coefficients $\gamma_1, \gamma_2, \ldots$ of an analytical expression for the AECs of the arc furnace (which are variable parameters for optimum control synthesis).

6. OPTIMAL CONTROL SYNTHESIS MODELS FOR CS

We now determine the family of particular optimum criteria and compose a control target functional for the entire system in order to perform the operative synthesis of the optimum control of an EAF electrical regime according to current (technological, industrial, energetic, etc.) external conditions and the required technical and economic indices.

One of the versions of the mathematical optimization model is a multicriterion multiparametric optimization based on the set of alternative Pareto's optimum solutions,

$$\Phi(\vec{x}) = \Phi(Q_1(\vec{x}), Q_2(\vec{x}), \ldots, Q_\nu(\vec{x})) = \sum_{i=1}^{\nu} \lambda_i Q_i(\vec{x}) \Rightarrow \min,$$

where:

$Q_1(\vec{x}), Q_2(\vec{x}), \ldots, Q_\nu(\vec{x})$ – partial criteria;

λ_i – their weight coefficients.

This functional determines a control target and, along with the vector $\vec{x}$ of variable setting system actions and the description of its variation range $\vec{x} \in D$, forms a mathematical model for decision making in the problem of the optimum multicriterion control strategy.

One of the challenges in increasing the level of the electromagnetic compatibility is the synthesis of optimum control based on an indirect criterion, namely, the sum of the dispersions of the normalized arc current $D^{*}_{I_a}(U_{a\,set}, \gamma)$ and the furnace reactive power $D^{*}_{Q}(U_{a\,set}, \gamma)$. The extremum of this criterion corresponds to the minimum of the dispersion of the network voltage fluctuational component.

$$D^{*}(U_{a.set}, \gamma) = \lambda_{I_a} D^{*}_{I_a}(U_{a.set}, \gamma) + \lambda_{Q} D^{*}_{Q}(U_{a.set}, \gamma) \Rightarrow \min, \qquad (2)$$

where:

λ_{I_a}, λ_{Q} – weight coefficients of the $D^{*}_{I_a}$, D^{*}_{Q} dispersions, respectively.

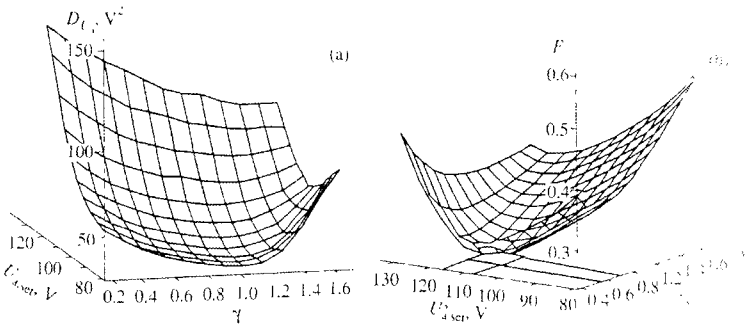

Fig. 3. Dependences of (a) the network-voltage dispersion and (b) the value of functional (3) on the setting actions of the two-circuit electrical-regime control system of a DSP-6 furnace.

Fig. 3a shows the dependence of the network voltage dispersion D_{I_a} on the variable setting actions of the system, namely, the EPCS arc-voltage setting and the AEC forming coefficient γ, which is obtained when the DSP-6 furnace regime is controlled by functional (2). The coordinates of its minimum determine the optimum setting actions $U^{*}_{a\,set}$ and γ^{*} of the two-circuit system when the electrical regime of the arc furnace is controlled by functional (2).

Another approach is the optimum-compromise control using the criterion of the maximum electric-power efficiency. This approach is effective due to the modern conditions of deficient and expensive electric power and the tendency toward intensifying a heat via an increase in the furnace transformer specific power (i.e., an increase in the secondary voltage of the transformer). This control can be synthesized using, e.g., the generalized additive functional

$$\begin{aligned}\Phi(U_{a\,set}, \gamma) = 0.28(1 - \overline{P}^{*}_{a}(U_{a.set}, \gamma) + 0.24\overline{P}^{*}_{ep}(U_{a\,set}, \gamma) \\ + 0.21 D^{*}_{I_a}(U_{a\,set}, \gamma) + 0.27\overline{W}^{*}(U_{a\,set}, \gamma)) \Rightarrow \min\end{aligned}. \qquad (3)$$

Fig. 3b shows the surface of this functional, and its extremum coordinates $U^{*}_{a\,set}$, γ^{*} correspond to the setting actions of the system when the optimum control is realized according to the maximum efficiency of using electric power.

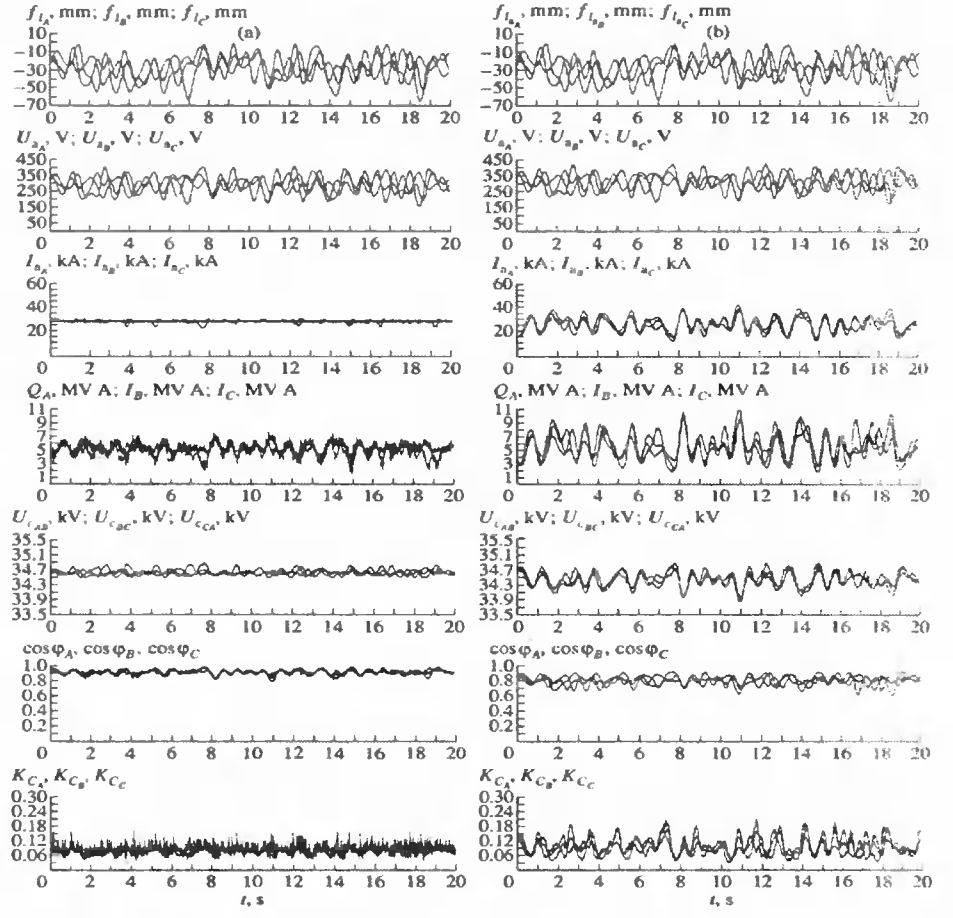

Fig. 4. Diagrams for DSP-50 electrical-regime coordinates at the stage of well melting for the operation of (a) the two-level CS and (b) an ARDG controller.

Control synthesis based on the formation of arc-furnace AECs of type *4* in Fig. 2 is an effective approach to optimizing furnace regimes according to the criterion of the maximum electric-power efficiency. A positive specific feature of characteristics of this type for this criterion is a minimum decrease in the arc power for medium-length arcs (in the range of rational furnace regimes) and an effective decrease in the power of the electric loss and the reactive furnace power for short arcs (for operational short circuits and similar regimes). As a result, the specific electric power consumption decreases, the reactive power consumption decreases, and the electric efficiency of an arc furnace increases.

We designed a hierarchic two-level system for the optimum control of the consumption regimes of the arc-furnace reactive power in order to substantially increase the electrical and technical efficiency of heat control and to improve the electromagnetic compatibility of arc-furnace regimes and power-network regimes. As an FRCCS, the lower level uses a high-speed subsystem for optimum reactive furnace power stabilization, which is optimized using criterion (2). In the general case, the upper level employs a static thyristor reactive power compensator. However, our results demonstrate that,

for low- and medium-power furnaces, the upper level can contain only a capacitor bank to compensate for the constant component of the reactive power, i.e., to increase the power coefficient to the required level. This increase is necessary to decrease the electrical losses in the furnace power circuit and the energy system. This is possible owing to the fact that the use of the optimum stabilization of the reactive furnace power in the lower level of the subsystem minimizes the fluctuational component of the reactive furnace power to a level at which network voltage oscillations, which are estimated from the flicker dose, do not exceed the normative values.

Table 1. Integrated indices for ARDG controller and proposed CS.

Index	Two-level CS	ARDG controller
$\overline{U}_a$, V	299.4	313.0
$\overline{I}_a$, kA	29.1	27.3
D_{I_a}, kA^2	0.939	35.4
$\overline{P}_a$, MW	7.05	6.73
$\overline{U}_n$, kV	34.67	34.46
D_{U_n}, $\times 10^3$ V^2	7.27	37.58
$\overline{I}_n$, A	330.2	353.1
$\overline{Q}_c$, MVA	5.26	5.61
D_Q, MVA^2	859	3354
$\overline{\cos(\varphi)}$	0.914	0.80
$\overline{K}_{n_{I_n}}$	0.0835	0.0971
δU_n, %	0.947	1.542
F	0.0379	0.220

The efficiency of the designed CS structures and the proposed strategies of the multicriterion control of the electrical regimes of the heat were tested using a digital instantaneous-coordinate model for the power system and the two-circuit control system for arc-furnace electrical-regime coordinates. We studied furnaces of various capacities at various heat stages. To adequately simulate electrical regimes at various stages, we used random arc-length fluctuations, whose statistical characteristics (in particular, a spectral perturbation density function along an arc) corresponded to the real characteristics of these fluctuations at a certain heat stage in an arc furnace.

As an example, Fig. 4 shows the calculated diagrams for the working parameters of a DSP-50 arc furnace and its power network at the stage of well melting for the reactive power consumption regime determined by the designed two-level CS during the operation of an ARDG standard electrohydraulic arc-power controller. For each phase, these diagrams show a perturbation variation along the arc length $f_{l_a}(t)$ at this stage of

heat, the arc voltage $U_a(t)$, the arc current $I_a(t)$, the furnace reactive power $Q(t)$, the voltage across the power-network busbars $U_n(t)$, the power factor $\cos\varphi(t)$, and the current harmonicity perturbation coefficient $K_h(U_a)$. The table gives the integrated indices (mathematical expectations, dispersions) that illustrate the operation efficiency of these systems and are obtained by the statistical processing of the results shown in Fig. 4. In these experiments, the arc voltage was $U_{a.set} = 313$ V, and an ARDG arc-power controller was used. As a result of the calculations, the nominal arc current is $I_a = I_{a\,n} = 27.3$ kA, and the arc power is $P_a = P_{a.n} = 6.73$ MW at a secondary voltage of 407 V. For the two-level CS, the secondary transformer voltage was increased by 10%, and the artificial external furnace characteristic was synthesized by functional (2) under conditions of a network voltage dispersion minimum. This minimum corresponds to the following optimum values: $\gamma^* = 0.75$ and $U_{a.set} = 299$ V.

The calculated integrated indices demonstrate that all of the indices are significantly improved when the two-level CS is used instead of an ARDG-type arc-power controller. For example, the arc-current dispersion decreases by 30-40 times, and the flicker dose F decreases by a factor of five to six. The loading current harmonic distortions coefficient decreases by 14-15%; the power factor increases by 14-15%; the arc power increases by 4-5%; and the deviation of the voltage across furnace busbars from the nominal voltage decreases by 1.4-1.6%.

7. CONCLUSIONS

The use of a high-speed subsystem that controls the resistance of a reactor involved in the power circuit of the primary winding of a furnace transformer in the structure of a proposed two-circuit CS allows one to realize the multicriterion optimum control of an EAF electrical regime. This control provides a substantial increase in the electrical and technical efficiency of arc-furnace regimes and improves the indices of the electromagnetic compatibility of the furnace and its power system.

The proposed two-circuit CS can be used to run heats at the minimum number of switchings of a furnace transformer, which decreases the heat time and increases the reliability of the furnace power supply. Variable setting actions for the realization of the multi-criterion optimum control in this case, i.e., at U_{2p}= const, are only represented by a preset arc voltage $U_{a\,set}$ and an $I_a(U_a)$ AEC relation for an arc furnace.

The substantial induced decrease in the amplitude and dispersion of the arc-current and furnace reactive power oscillations decreases the flicker dose by a factor of five to six and decreases the electrodynamic forces in the elements of the electric power facilities and their mechanical vibrations. As a result, the reliability of this equipment increases.

Efficiency of optimal control strategies implementation increased due to their synchronization with changes of melting stages, which are identified by hierarchical neural-network based control system.

BIBLIOGRAPHY

[1] 2005. Eighth International Conference on Steel Electrometallurgy (Part 1), Elektrometallurgiya, No. 12, 36-43.
[2] Gudim Yu.A., Zinurov I.Yu., Kiselev A.D., Shumakov A.M., 2005. Rational Methods for Heat Intensification in Modern Arc Steelmaking Furnaces. Elektrometallurgiya, No. 9, 2-6.
[3] Andrianova A.Ya., Paranchuk Ya.S., Lozinskii A.O., 2004. Some Problems of Intelligent Control in Arc Steel-making Furnaces. Elektrometallurgiya, No. 3, 30-37.
[4] Bedin M., Romano M., 2004. Arc Furnace Powered through a Saturating Reactor. Elektrometallurgiya, No. 4, 15-20.
[5] Lozinskii A.O., Paranchuk Ya.S., 2008. Kohonen neural network synthesis for melting stages recognition in arc steel furnace. Proceedings of conference Artificial intelligence and intelligent systems. Donetsk: IPI 2008, T1, 124-129.
[6] Paranchuk R.Ya., 2008. Neural-network based system of optimal electrical mode coordinates stabilization in arc steel-melting furnace. Proceedings of conference Simulation, identification and synthesis of control system MISSU'2008. Moscow-Donetsk, 177-178.

ENERGOOSZCZĘDNY, WIELOKRYTERIALNY UKŁAD INTELIGENTNY DO STEROWANIA ELEKTRYCZNYMI STANAMI PRACY PIECA ŁUKOWEGO DO TOPIENIA STALI

Streszczenie

W artykule zaproponowano hierarchiczną strukturę układu adaptacyjnego do wielokryterialnego sterowania stanami pracy trójfazowego pieca łukowego do topienia stali. Opracowano modele syntezy optymalnego wektora sterowania. Adaptacja sterowania dokonuje się w zależności od stadiów technologicznych topienia stali, które są identyfikowane za pomocą sieci neuronowej.

Słowa kluczowe: piec łukowy do topienia stali, sieć neuronowa, układ sterowania

UNIWERSYTET TECHNOLOGICZNO-PRZYRODNICZY
IM. JANA I JĘDRZEJA ŚNIADECKICH W BYDGOSZCZY
ZESZYTY NAUKOWE NR 254
ELEKTROTECHNIKA 14 (2009), 17-24

COMPUTER SIMULATION OF THE ELECTROMECHANICAL SYSTEMS USING CONVOLUTION INTEGRAL

Volodymyr Moroz

National University "Lviv's Politechnic"
Institute Power Energy and Control System
Bandera Str., 12, Lviv-13, 79646, Ukraine.
e-mail: vmoroz@polynet.lviv.ua

Summary: The method of the computer simulation of the electromechanical systems using the recurrent equations based on the convolution integral approximations is presented in the paper.

Keywords: electromechanical system, computer simulation, convolution integral, ordinary differential equation (ODE)

1. INTRODUCTION

The numeric methods for solving the ordinary differential equations (ODEs) are used for the computer simulations of the electromechanical systems widely. There are no problems to solve the systems of the ODEs with smooth or low varying solutions but problems appear when solutions are complicated with the very fast components of the process. The example to show these problems using well-known environment MATLAB with Simulink can be found in [1] – the different methods give the different results and automatic step control can't to improve this situation.

Different solutions obtained by means of different numeric methods intended for solving ODEs with the automatic step control strategy were described in [2] also as example for MATLAB ODEs suit (*only for second-order system of equations*!).

This phenomenon of ODEs solution using the numeric methods is the consequence of their basic principle – all numeric methods for solving the ODEs approximate the solution by the limited Taylor series that is suitable for continues smooth functions only. As the result the modern electromechanical system with power pulse-width modulation (PWM) can't be correct simulated using the traditional numeric methods because their signals are interrupted (discontinues). Such problem can be solved using analytic or integration-based methods some of which are based on the convolution integral [3].

2. FUNDAMENTALS

The proposed method based on the convolution integral approximation that produces simple but effective recurrent modelling equations [3], [4]. Some problems can be solved using presented approach:

- Numerical stability – the theorem of the strong numeric stability of this formulas was proved in [4];
- Simplicity of the obtained recurrent formulas – they are simple and comprehensible;
- Obtained equations are very effective – the operating step during the computer simulation is limited by the Shannon's sampling theorem.

The proposed method is based on the two principles:

1) The modelling object's transient behaviour is defined and described by the one of the common methods:
   - system of ODEs;
   - transfer function W(s);
   - structured model etc,

   and can be decomposed to the elementary dynamic blocks (*this method called as the parallel decomposition*).
2) The free input signal or excitation $x(t)$ of the modelled system is undefined symbolically that's must be approximated by the polynomial $x^*(t)$ using signal samplings. This principle is used in z-transform on the basis of zero- and first-order approximation for the sampled signals [5].

The output (response) of the dynamic system can be described by the convolution integral in the following form:

$$y(t) = y_0(t) + \int_0^t x(\tau) \cdot w(t-\tau)\, d\tau,$$

where:

$y(t)$ – output system response;
$y_0(t)$ – system response for nonzero initial conditions;
$x(t)$ – system input or excitation;
$w(t)$ – impulse response of the system, corresponds to the inverse Laplace transform of the system transfer function $W(s)$.

The system response for nonzero initial conditions $y_0(t)$ can be written it was shown [3]:

$$y_0(t) = \mathrm{L}^{-1}\left(\frac{\sum_{j=1}^{n} \left(y_0^{(j-1)} \sum_{i=j}^{n} a_i s^{i-j} \right)}{A(s)} \right),$$

where:

L – Laplace transform;
n – system transfer function $W(s)$ order;
$y_0^{(j)}$ – j^{th} derivative of the $y_0(t)\Big|_{t=0}$;
$A(s)$ – polynomial denominator of the system transfer function $W(s)$;
a_i – polynomial coefficients of the denominator $A(s)$.

The final equation of the system response with the nonzero initial conditions is

$$y(t) = \mathrm{L}^{-1}\left\{ \frac{\sum_{j=1}^{n}\left(y_0^{(j-1)} \sum_{i=j}^{n} a_i s^{i-j} \right)}{A(s)} \right\} + \int_0^t x(\tau) \cdot w(t-\tau)\, d\tau .$$

The main problem of the convolution integral calculation is the missing of the analytic description of the input signal $x(t)$, because it is free of decision usually. For example, the input of the actuator or controller in the closed automatic system is unknown (undetermined) as the result there is no analytic description of the input $x(t)$ for convolution integral calculation. This problem can be solved by the polynomial approximation of the sampled signal $x^*(t)$.

There are two ways to create the polynomial approximation $x^*(t)$:

1) the **explicit** rule that use current (index "i") and previous samples of the data – only this principle can be applied in the real-time systems;
2) the **implicit** rule that uses the next (index "$i+1$") and the current and previous (when are need) samples of the data – this principle may be apply for the computer simulation because implicit equations can be solved by the analytic or numeric method.

There are simple examples below illustrate the basic of the polynomial approximation: the coefficients of the first-order approximation polynomial $x^*(t) = a_1 \cdot t + a_0$ can be finding with two samples as shown below.

From explicit rule:

Coefficients using samples x_{i-1} and x_i on the discrete time t_{i-1} i t_i can be finding from the following set of equations:

$$\begin{cases} a_0 = x_i ; \\ -a_1 \cdot h + a_0 = x_{i-1} ; \end{cases} \Rightarrow \begin{cases} a_0 = x_i ; \\ a_1 = \dfrac{x_i - x_{i-1}}{h}. \end{cases}$$

From implicit rule:

Coefficients using samples x_i and x_{i+1} on the discrete time t_i i t_{i+1} can be finding from the other system of equations:

$$\begin{cases} a_1 \cdot h + a_0 = x_{i+1} ; \\ a_0 = x_i ; \end{cases} \Rightarrow \begin{cases} a_0 = x_i ; \\ a_1 = \dfrac{x_{i+1} - x_i}{h}. \end{cases}$$

There are polynomials of any order can be build using those rules but their high orders are not optimal for the signal reconstruction.

The analysis of the rational polynomial approximation order based on the classic control theory which operate by the Bode's diagrams of the investigating system. So, we can describe the polynomial as discrete filter and build discrete transfer function for it. The Bode analyse in such case is based on two rules:

- Equation $X_i = \frac{1}{h}\int_{t_i}^{t_{i+1}} x(t)\,dt$ corresponds to analytic integration which Laplace transform is $\frac{1}{s}$ and Bode's diagram build from the frequency-based form $\frac{1}{j\cdot\omega}$.
- Equation $X_i^* = \frac{1}{h}\int_{t_i}^{t_{i+1}} x^*(t)\,dt$ corresponds to integral of the approximation polynomial.

That's polynomial approximation errors using Bode analyse is the result of the research of the frequency errors between ideal integrator and its approximation by integration of the polynomial $x^*_{(n)}(t) = a_n t^n + ... + a_2 t^2 + a_1 t + a_0$:

$$\varepsilon_i = X_i - X_i^* = \frac{1}{h}\int_{t_i}^{t_{i+1}} x(t)\,dt - \frac{1}{h}\int_{t_i}^{t_{i+1}} x^*(t)\,dt = \frac{1}{h}\int_{t_i}^{t_{i+1}} \left(x(t) - x^*(t)\right)dt .$$

The high frequency for the Bode analysis depends on Shannon's sampling theorem and it is twice lower than the sampling frequency ω_0. The operational frequency ω for the most digital systems such as the computer models is lower than sampling frequency ω_0 ten times at least. The resulted Bode diagrams of the frequency errors of the polynomial approximations relative ideal integration are shown on Figure 1 [3]. The rational order of the polynomial approximation is not high than 3 but the 1st order implicit approximation produces better result because it is simple without phase errors.

The whole system impulse response $w(t)$ has the Laplace transformation $W(s)$ that can be decomposed on the poles and zeros using Heaviside theorem. So, the complete convolution integral can be represented as the sum of the convolution integrals of the k decomposed elementary parts:

$$y(t) = y_0(t) + \int_0^t x(\tau)\cdot w(t-\tau)\,d\tau = \sum_{k=1}^{N} y_{0k}(t) + \sum_{k=1}^{N}\int_0^t x(\tau)\cdot w_k(t-\tau)\,d\tau .$$

The real poles are the universal representation of the set of poles because zero pole (integrator) is the particle occasion of the real pole for example and corresponds to ordinary differential equation. The pair of the complex poles can be represented as the connection of the real and zero poles [5] that can be describe by the two first order differential equations:

$$T^2 y'' + 2\xi T y' + y = x \quad \Rightarrow \quad \begin{cases} y' = z ; \\ \dfrac{T}{2\xi} z' + z = \dfrac{x - y}{2T\xi} . \end{cases}$$

This way reduces accuracy slightly (*that can be compensated by small step size reducing*) but simplifies obtained recurrent equations very much [5].

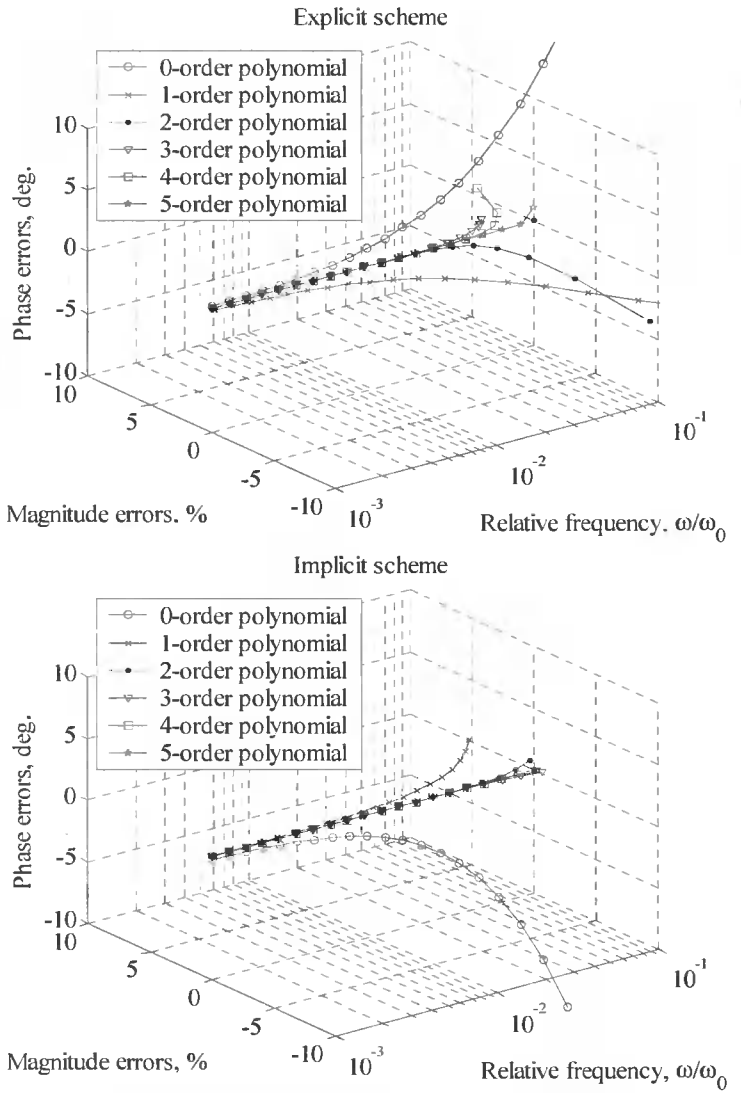

Fig. 1. Bode's plots of the polynomial approximation of the sampled signal.

The impulse response of the block with the real pole is the fading exponent $w_1(t) = \frac{1}{T} e^{-\frac{h}{T}}$ where h is the time step and T corresponds to the real pole. The first order **explicit** polynomial approximation used for signal approximation $x^*(t)$ produces response of first-order pole for nonzero initial conditions and free input as the result:

$$y_1(t) = y_{0_1}(t) + \int_0^t x^*(\tau) \cdot w_1(t-\tau)\, d\tau = \mathrm{L}^{-1}\left(\frac{y_0 \cdot T \cdot s}{T \cdot s + 1}\right) + \int_0^t (a_1 \cdot \tau + a_0) \cdot \frac{1}{T} e^{-\frac{t-\tau}{T}}\, d\tau =$$

$$= y(0) \cdot e^{-\frac{t}{T}} + \frac{1}{T} \int_0^t \left(\frac{x_t - x_{t-1}}{h}\tau + x_t\right) e^{-\frac{t-\tau}{T}}\, d\tau.$$

Let us replace t by h and calculate integral on time distance $t_t \le t < t_{t+1}$ we obtain the explicit modelling recurrent formula after the simple algebra conversation:

$$y_{t+1} = y_t e^{\frac{-h}{T}} + \left(1 - e^{\frac{-h}{T}}\right) \cdot x_t + \left(1 - \frac{T}{h}\left(1 - e^{\frac{-h}{T}}\right)\right) \cdot (x_t - x_{t-1}).$$

Using the first order **implicit** polynomial approximation (the best choice for author view – see [3]) used for signal approximation $x^*(t)$ produces the other form of the response:

$$y_1(t) = y_{0_1}(t) + \int_0^t x^*(\tau) \cdot w_1(t-\tau)\, d\tau = \mathrm{L}^{-1}\left(\frac{y_0 \cdot T \cdot s}{T \cdot s + 1}\right) + \int_0^t (a_1 \cdot \tau + a_0) \cdot \frac{1}{T} e^{-\frac{t-\tau}{T}}\, d\tau =$$

$$= y(0) \cdot e^{-\frac{t}{T}} + \frac{1}{T} \int_0^t \left(\frac{x_{t+1} - x_t}{h}\tau + x_t\right) e^{-\frac{t-\tau}{T}}\, d\tau.$$

As the result we obtain the implicit modelling recurrent formula:

$$y_{t+1} = y_t e^{\frac{-h}{T}} + x_{t+1} - x_t e^{\frac{-h}{T}} - \frac{T}{h}(x_{t+1} - x_t)\left(1 - e^{\frac{-h}{T}}\right).$$

Those formulas types (explicit and implicit) are using for computer simulation based on traditional prediction-correction rules [2]

3. EXAMPLES

The proposed method was tested on the complicated electromechanical object as electric drive system that describe by the 10^{th} order system of the nonlinear ODEs – this is the 2-motor 3-mass electric drive system of the swing drive of the power mining shovel

Fig. 2. Nonlinearities of the ODE's system are:

- the saturation of the controllers;
- the static and dynamic nonlinearities of the thyristor exciter;
- magnetic saturation of the DC generator;
- air gaps in the mechanical part of the swing drive.

Simulation results for this model are shown in the Fig. 3 (electric drive voltage and current) and Fig. 4 (the shaft torques).

Computer simulation time on the time interval 6 s for the proposed formula with the fixed time step 10 ms (*emulate discrete properties of the DC' generator thyristor*

exciter) was 0.13 s using MATLAB environment on Intel Celeron-1400 processor and over 25 s and more for the standard MATLAB functions for ODEs – ode23, ode45 and ode113. The MATLAB functions for the stiff ODEs didn't work properly because gaps were presented in the mechanical joints.

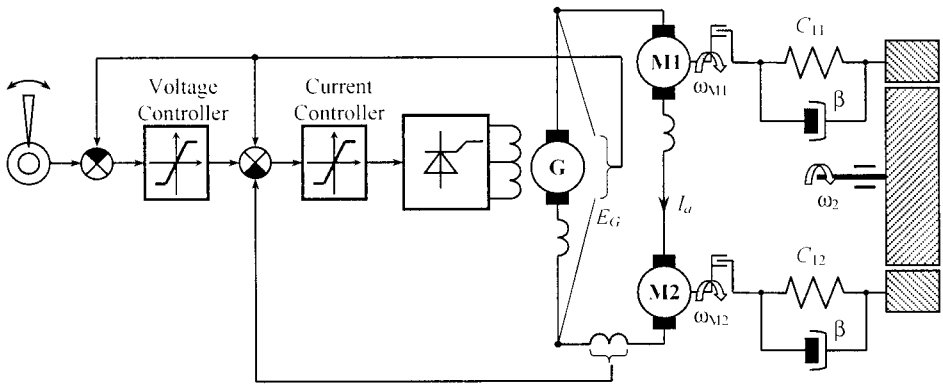

Fig. 2. Two-motors 3-mass electric drive system for the swing drive of the power mining shovel.

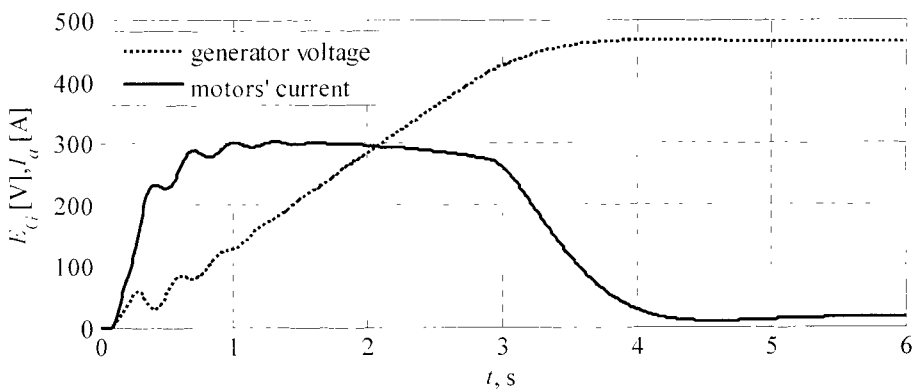

Fig. 3. Generator voltage and motors' current for electric drive model.

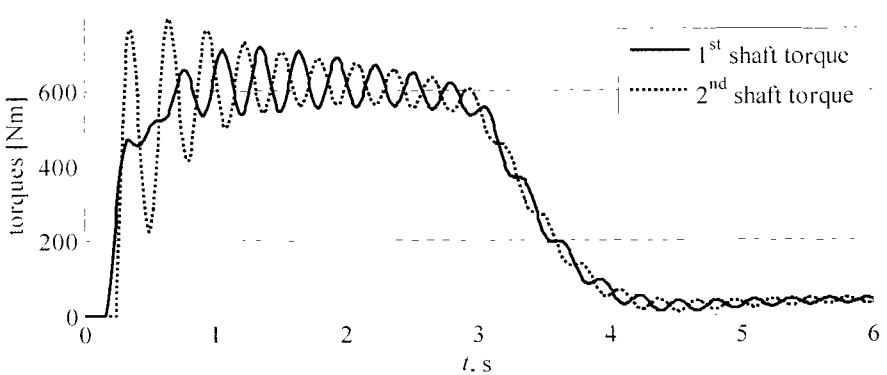

Fig. 4. Shafts' torques for swing drive of the power mining shovel.

The root-mean-square (RMS) relative errors of the proposed formula weren't higher than 1.65% for the torques, no more 0.86% for the motors' current and were less than 0.27% for the angular velocities comparing to any MATLAB numeric methods for ODEs with 10^{-6} tolerance.

4. CONCLUSIONS

The proposed approach is suitable for various problems solution in the field of electrical engineering. Main advantages of proposed method are:

- obtained modelling equations are numerically stable and don't dependent on the step size;
- the proposed approach produce quit simple but effective equations that are suitable for simulation of linear and nonlinear dynamic objects;
- the proposed method is suitable for the real-time computer simulation and produces the effective recurrent modelling formulas with the good tolerance.

BIBLIOGRAPHY

[1] Мороз В., 2005. Особливості застосування числових методів у моделюванні сучасних електроприводів. Теоретична електротехніка. Вип. 58, 130-137.
[2] Shampine L., Reichelt M. The MATLAB ODE Suite: http://www.mathworks.com/access/helpdesk/help/ pdf_doc/otherdocs/ode_suite.pdf
[3] Moroz V., 2008. The Numerically-Analytic Method for the Real-Time Computer Simulation. 9th International Workshops "Computational Problems of Electrical Engineering" (under auspices IEEE). Alushta (Crimea), Ukraine, 162-164.
[4] Мороз В., 2007. Ефективні рекурентні формули для комп'ютерного моделювання електромеханічних систем. Вісник Національного університету „Львівська політехніка". Електроенергетичні та електромеханічні системи. № 597, 3-11.
[5] Moroz V., 2005. High-Speed Precise Simulation Using Modified Z-Transform. Proceedings of the XIII International Symposium on Theoretical Electrical Engineering ISTET'05. Lviv, Ukraine, 184-186.

SYMULACJA KOMPUTEROWA UKŁADU ELEKTROMECHANICZNEGO Z WYKORZYSTANIEM CAŁKI SPLOTU

Streszczenie

W artykule przedstawiono metodę symulacji komputerowej układu elektromechanicznego z wykorzystaniem równań rekurencyjnych opartych na aproksymacji całki splotu.

Słowa kluczowe: układ elektromechaniczny, symulacja komputerowa, całka splotu, układ równań różniczkowych

UNIWERSYTET TECHNOLOGICZNO-PRZYRODNICZY
IM. JANA I JĘDRZEJA ŚNIADECKICH W BYDGOSZCZY
ZESZYTY NAUKOWE NR 254
ELEKTROTECHNIKA 14 (2009), 25-36

THE RECOVERY METHOD FOR PROPER ENVELOPE COMPLEX DISTORTIONAL AMPLITUDE MODULATED SIGNAL BASED ON HILBERT TRANSFORM

Sławomir Andrzej Torbus

University of Technology and Life Sciences
Al. S. Kaliskiego 7, 85-796 Bydgoszcz
e-mail: slator@utp.edu.pl

Summary: In this paper the definition of Hilbert transform and analytical representation of the signal are presented. The method of determining the envelope of amplitude modulated signals using Hilbert transform is defined. The article discusses the benefits of this method with the use of radio transmission, which are affected by the interference from low frequency signals the source of which may be a network of electricity. This subject is supported by specific examples.

Keywords: Hilbert transform, analytic signal, amplitude modulated signal, the signal envelope

1. INTRODUCTION

In the transmission radio systems analogue and digital information have to be modulated. Demodulated signal is sent in the form of high frequency electromagnetic radio wave from a transmitter to a receiver where signal is demodulated and information is recovered. Assuming that the carrier signal is purely cosine after modulation it can be described as follows [1]:

$$s(t) = a(t) \cdot \cos\left(2 \cdot \pi \cdot f_c(t) \cdot t + \varphi(t)\right) \tag{1}$$

where:

$a(t)$ – amplitude of signal,

$f_c(t)$ – frequency of signal,

$\varphi(t)$ – phase of signal.

Depending on the identified parameters of the signal (1) changes over time, we can distinguish the following types of modulation: the **amplitude modulation** where the amplitude is modulated, the **frequency modulation**, if the frequency is modulated, and the **phase modulation** if the phase is modulated.

One of the basic and frequently used types of modulation is amplitude modulation, determined at a glance AM (Amplitude Modulation), which relies the changes of amplitude of the signal during the prescribed pattern (1) with predetermined values of fre-

quency $f(t)$ and phases $\varphi(t)$ this signal. However, it must be added that the simplicity of the implementation of the amplitude modulation entails some disadvantages, such as the lack of resistance to interference of various kinds, among which the impact of low frequency signals stemming from the electricity network can be distinguished. Therefore, the discussed disturbances – distortions have an adverse effect on the modulated signal, causing the modulating signal of low frequency around 50 Hz – the frequency of electricity network in Poland. As the consequence of these distortions the faulty reception on the receiving side appears, which results in errors in transmission.

According to the definition and properties of the amplitude modulation, the modulated signal (1) is a narrowband signal, because it satisfies the assumption that the baseband of this signal is a small relative to the carrier frequency signal. Such a complex analysis can be used for the representation of narrowband signals. With respect to the modulated signal (1), after applying the formulas of trigonometric functions of angles and determining the amount of unchanged in time frequency $f_c(t) = f_c = const$ we get:

$$\begin{aligned} s(t) &= a(t)\cdot\cos\left(2\cdot\pi\cdot f_c\cdot t+\varphi(t)\right)= \\ &= a(t)\cdot\cos\left(\varphi(t)\right)\cdot\cos\left(2\cdot\pi\cdot f_c\cdot t\right)+ \\ &-a(t)\cdot\sin\left(\varphi(t)\right)\cdot\sin\left(2\cdot\pi\cdot f_c\cdot t\right)= \\ &= x(t)\cdot\cos\left(2\cdot\pi\cdot f_c\cdot t\right)-y(t)\cdot\sin\left(2\cdot\pi\cdot f_c\cdot t\right) \end{aligned} \tag{2}$$

where:

$x(t)$ and $y(t)$ – the quadrature components of signal $s(t)$, which using the pattern (2) can be defined as $x(t)=a(t)\cdot\cos(\varphi(t))$ - the synphase component of signal $s(t)$, $y(t)=a(t)\cdot\sin(\varphi(t))$ – the quadrature component of signal $s(t)$. Using these components we can find the signal envelope:

$$\underline{z}(t)=x(t)+j\cdot y(t)=a(t)\cdot\cos(\varphi(t))+j\cdot a(t)\cdot\sin(\varphi(t))=a(t)\cdot e^{\varphi(t)} \tag{3}$$

While analyzing the modulated signal (1) it can be deduced that the complex carrier signal has the following form:

$$\underline{c}(t)=\cos\left(2\cdot\pi\cdot f_c\cdot t\right)+j\cdot\sin\left(2\cdot\pi\cdot f_c\cdot t\right)=e^{j\cdot 2\cdot\pi\cdot f_c\cdot t} \tag{4}$$

Making a composite complex carrier multiplication (4) and the envelope complex (3) we obtain:

$$\begin{aligned} \underline{c}(t)\cdot\underline{z}(t) &= e^{j\cdot 2\cdot\pi\cdot f_c\cdot t}\cdot\left[a(t)\cdot\cos\left(\varphi(t)\right)+j\cdot a(t)\cdot\sin\left(\varphi(t)\right)\right]= \\ &= e^{j\cdot 2\cdot\pi\cdot f_c\cdot t}\cdot a(t)\cdot e^{j\cdot\varphi(t)}=a(t)\cdot e^{j\left(2\cdot\pi\cdot f_c\cdot t+\varphi(t)\right)}= \\ &= a(t)\cdot\left[\cos\left(2\cdot\pi\cdot f_c\cdot t+\varphi(t)\right)+j\cdot\sin\left(2\cdot\pi\cdot f_c\cdot t+\varphi(t)\right)\right]= \\ &= a(t)\cdot\cos\left(2\cdot\pi\cdot f_c\cdot t+\varphi(t)\right)+j\cdot a(t)\cdot\sin\left(2\cdot\pi\cdot f_c\cdot t+\varphi(t)\right) \end{aligned} \tag{5}$$

When comparing the formula (1) with the formula (5) a very important relationship can be noticed, namely, that the modulated signal $s(t)$ is the real part of the composite multiplying complex carrier signal $\underline{c}(t)$ by the complex envelope $z(t)$:

$$s(t) = \mathrm{Re}[\underline{c}(t) \cdot z(t)] \tag{6}$$

This analysis allows us to conclude that on the receiving side the received data can be decoded successfully without errors, when we have to get complex envelope of modulated signal. For this purpose, we use the Hilbert transform, which gives a quadrature component, which is the imaginary part of the complex envelope of the analyzed signal.

I would add that the application of Hilbert transform in signal processing can be found in the literature following sources: Zieliński P. T.: *Cyfrowe przetwarzanie sygnałów. Od teorii do praktyki.* WKŁ, Warszawa 2007, Wetula A.: *Zastosowanie transformaty Hilberta do wyznaczania obwiedni zespolonej napięć i prądów sieci elektroenergetycznej.* AGH Kraków, Oczeretko E., Borowska M., Laudański M.: *Przekształcenie Hilberta w przetwarzaniu sygnałów i obrazów biomedycznych.* Uniwersytet w Białymstoku. Analyzing sources of literature I can say that I have examined the problem is new, so devoted to him this publication.

2. DEFINITION AND PROPERTIES OF AMPLITUDE MODULATION

Assume that the carrier wave has the cosine character and is defined as follows:

$$c(t) = U_{c_m} \cdot \cos(2 \cdot \pi \cdot f_c \cdot t + \varphi_c) \tag{7}$$

where:

U_{c_m} – the amplitude of carrier wave;

f_c – the frequency of carrier wave;

φ_c – the phase of carrier wave.

The changes of carrier wave are made according to parameters of modulating wave, represented by the pattern:

$$m(t) = U_{m_m} \cdot \cos(2 \cdot \pi \cdot f_m \cdot t + \varphi_m) \tag{8}$$

where:

U_{m_m} – the amplitude of modulating wave;

f_m – the frequency of modulating wave;

φ_m – the phase of modulating wave.

Consequently, the instantaneous value of the amplitude modulated signal can be described as follows:

$$a(t) = U_{c_m} + m(t) = U_{c_m} + U_{m_m} \cdot \cos(2 \cdot \pi \cdot f_m \cdot t + \varphi_m) = \\ = U_{c_m} \cdot \left(1 + \frac{U_{m_m}}{U_{c_m}} \cdot \cos(2 \cdot \pi \cdot f_m \cdot t + \varphi_m)\right) \tag{9}$$

Using amplitude modulation parameters, such as the sensitivity of the amplitude modulator and the ratio of modulation depth, the formula (9) can be expressed as follows:

$$a(t) = U_{c_m} \cdot \left(1 + k_a \cdot U_{m_m} \cdot \cos(2 \cdot \pi \cdot f_m \cdot t + \varphi_m)\right) = \\ = U_{c_m} \cdot \left(1 + m \cdot \cos(2 \cdot \pi \cdot f_m \cdot t + \varphi_m)\right) \tag{10}$$

where:

$k_a = \frac{1}{U_{c_m}}$ – the sensitivity of the amplitude modulator;

$m = \frac{U_{m_m}}{U_{c_m}}$ – the ratio of modulation depth.

Having the formula (1) the value of the instantaneous amplitude modulated signal, described by formulas (9) and (10), we can describe the amplitude modulated carrier signal:

$$s(t) = U_{c_m} \cdot \left(1 + m \cdot \cos(2 \cdot \pi \cdot f_m \cdot t + \varphi_m)\right) \cdot \cos(2 \cdot \pi \cdot f_c \cdot t + \varphi_c) \tag{11}$$

At this point it is worth mentioning that the envelope of amplitude modulated signal $s(t)$ will have the same shape as the modulating signal $m(t)$, if the following conditions will be fulfilled [2]:

- the amplitude of signal $k_a \cdot m(t) = k_a \cdot U_{m_m} \cdot \cos(2 \cdot \pi \cdot f_m \cdot t + \varphi_m)$ always has to be less then one, so $\forall t \in R : |k_a \cdot m(t)| < 1$. This condition guarantees, that the function $1 + k_a \cdot m(t) = 1 + k_a \cdot U_{m_m} \cdot \cos(2 \cdot \pi \cdot f_m \cdot t + \varphi_m)$ is always positive, therefore, the envelope of modulated signal is described by pattern (9). It could be considered a variant, when $\exists t \in R : |k_a \cdot m(t)| > 1$, the carrier wave is overmodulated, and consequently the reverse phase of the carrier wave at the points, where the function $1 + k_a \cdot m(t) = 1 + k_a \cdot U_{m_m} \cdot \cos(2 \cdot \pi \cdot f_m \cdot t + \varphi_m)$ is zero. However, when $\exists t \in R : |k_a \cdot m(t)| = 1$ then we have full modulation. An important suggestion is to protect the relation between the envelope of the AM wave, and the modulation wave all the time. That is why we have to select the appropriate value of the sensitivity of the amplitude modulator, or an appropriate ratio of modulation depth – typical of its value should be the range $m \in (0{,}2;0{,}8)$, in the audio systems this value should be in the range $m \in (0{,}3;0{,}5)$;
- the carrier frequency must be chosen in compliance with the transmission medium. When considering radio transmission, we can conclude that by reducing the frequency of the carrier signal frequency spectrum we can avoid the risk of overlapping

between the transmitted signals. The frequency range of radio wave is from 3 Hz to 3 THz, so the proper choice of carrier frequency signal is a signal of high frequency. The transmission of high frequency electromagnetic waves is simpler than low frequency electromagnetic wave. Thus, a carrier wave frequency f_c is much greater than that, which modulates the frequency f_m $(f_c >> f_m)$. The AM modulation bandwidth is defined as $W = 2 \cdot f_m$. This means that the amplitude modulated signal is a narrowband signal.

3. MATHEMATICAL MODEL AND SIMULATION OF THE INFLUENCE LOW FREQUENCY DISTORTION OF AMPLITUDE MODULATED SIGNAL

In this paper the influence of existing electromagnetic field induced by high voltage power lines is presented. For this purpose it is necessary to introduce the concept of distortion low frequency signal, which must be understood as a purely cosine signal, the frequency of which is approximately 50 Hz. The amplitude of this signal is low in relation to the amplitude modulated transmitted signal. In addition, it is worth mentioning that, as in the case of the signal, which modulates the carrier phase, it may be zero, that in case of distortion has not always phase have be zero, so we must take into consideration its change over time. This distortion will result not only in overmodulation amplitude of signal but also in the frequency of signal, still the frequency modulation is a very slow process.

The analysis will be incorporated into a clean signal modulation cosine, but more complex signals can be used too. An example of a complex signal may be an acoustic signal, with a very complicated process of defining the shape of the color and intensity of sound. This signal is the sum of multiple sinusoidal waveforms at fixed intervals, the frequency and amplitude of which change over time.

Considering the assumptions above, for the purposes of simulation we can take the following mathematical descriptions and determine the parameters of individual signals:

- carrier signal:

$$c(t) = U_{c_m} \cdot \cos(2 \cdot \pi \cdot f_c \cdot t) \tag{12}$$

where:

$U_{c_m} = 200$ mV,

$f_c = 10$ kHz;

- modulating signal:

$$m(t) = U_{m_m} \cdot \cos(2 \cdot \pi \cdot f_m \cdot t) \tag{13}$$

where:

$U_{m_m} = 160$ mV,

$f_m = 1$ kHz;

- amplitude modulated signal:

$$s(t) = (1 + k_a \cdot m(t)) \cdot c(t) = \\ = U_{c_m} \cdot (1 + k_a \cdot U_{m_m} \cdot \cos(2 \cdot \pi \cdot f_m \cdot t)) \cdot \cos(2 \cdot \pi \cdot f_c \cdot t) \tag{14}$$

where:

$$k_a = \frac{1}{U_{c_m}} = \frac{1}{200 \cdot 10^{-3}} = 5 \text{ V}^{-1};$$

- low frequency distortion:

$$n(t) = U_{n_m} \cdot \cos(2 \cdot \pi \cdot f_n \cdot t + \varphi_n(t)) \tag{15}$$

where:

$U_{n_m} = 80$ mV,

$f_n = 50$ Hz,

$\varphi_n(t) = \frac{\pi}{4} \cdot \cos(2 \cdot \pi \cdot (1 \text{ Hz}) \cdot t)$.

In accordance with the agreed objectives for the signals (12) and (13) can be obtained from a graph of function (14) describing the signal amplitude modulated with the envelope. It is a signal without low frequency distortion signal.

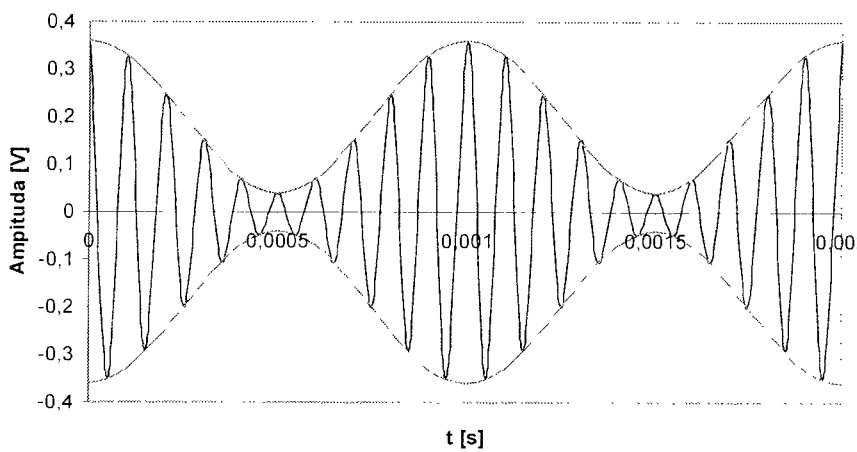

Fig. 1. Amplitude modulated signal $s(t)$ with envelope

A form of modulated carrier signal shown in Fig. 1, is without distortion and fully consistent with its mathematical description. In fact, transmitted signals are some obstacles that may make overmodulation signal $s(t)$. According to this assumption it can be stated that the modulated signal $s(t)$ will be the carrier signal, and the signal $n(t)$ representing the distortion will be the modulating one. Therefore, the mathematical representation of this situation will be as follows:

$$s_n(t) = \left(1 + k_{a_n}(t) \cdot n(t)\right) \cdot s(t) \tag{16}$$

where:

$k_{a_n}(t) = \dfrac{1}{U_{c_m} \cdot \left(1 + k_a \cdot U_{m_m} \cdot \cos(2 \cdot \pi \cdot f_m \cdot t)\right)}$ – instantaneous amplitude sensitivity, this parameter varies in time, because the amplitude of signal $s(t)$ varies in time.

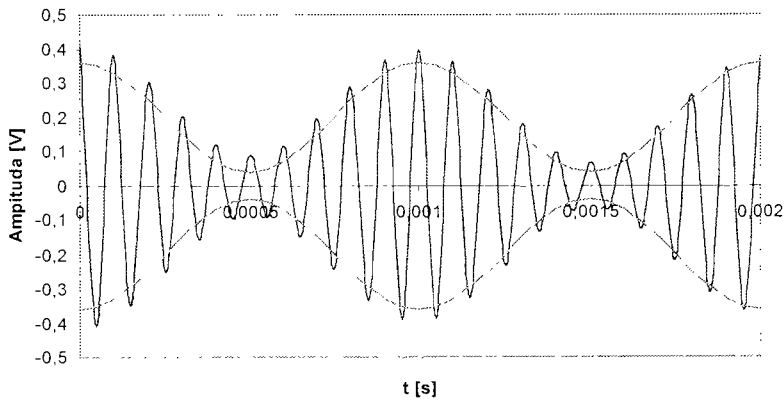

Fig. 2. Amplitude modulation signal with distortion $n(t)$ and with evolve of amplitude modulated signal $s(t)$

In Figure 2, we can see that the modulated signal does not contain the envelope. This confirms the correctness of the assumption that low frequency distortion has a significant impact on the transmission of amplitude modulated signals. It is necessary to develop appropriate methods for filtration in order to determine the correct carrier signal without distortions, which can be easily decoded.

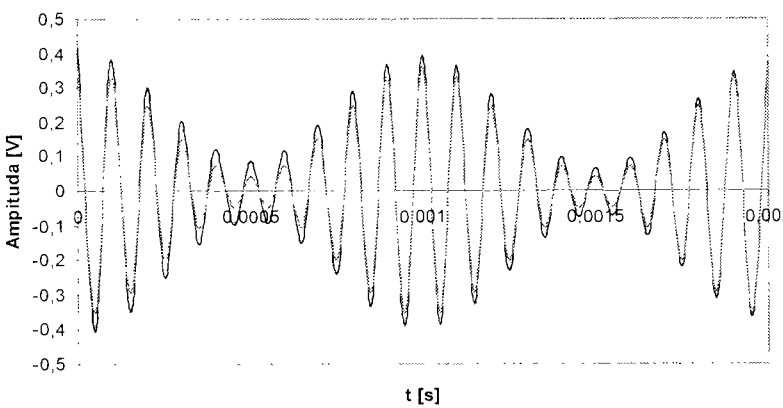

Fig. 3. Amplitude modulated signal with distortion $n(t)$ and amplitude modulated signal without distortion $s(t)$

4. DEFINITION, PROPERTIES AND APPLICATION OF HILBERT TRANSFORM

Hilbert transformation is defined by the operation of integration, which represents the signal studied in a different function. If the signal $x(t)$ is real, then if there is the Hilbert transform, it can be summarized as follows [1]:

$$\mathrm{H}\{x(t)\} = y(t) = x(t) * h(t) = x(t) * \frac{1}{\pi \cdot t} = \frac{1}{\pi} \cdot \int_{-\infty}^{+\infty} \frac{x(\tau)}{t-\tau} d\tau \tag{17}$$

where:

$h(t) = \frac{1}{\pi \cdot t}$ – impulse response filter, which gives moving phase about $\frac{\pi}{2}$ in the whole frequency range;

$*$ – convolution operation.

Knowing the Hilbert transform of a signal $x(t)$ can be determined composite analytical directly related to it. Its form is as follows:

$$z(t) = x(t) + j \cdot y(t) = x(t) + j \cdot \mathrm{H}\{x(t)\} = x(t) + j \cdot x(t) * h(t) \tag{18}$$

Using the Euler's identity to the pattern (18) we obtain a generalized form of the instantaneous amplitude and instantaneous phase of the composite signal $z(t)$. They are as follows:

$$a(t) = |z(t)| = \sqrt{x^2(t) + y^2(t)} = \sqrt{x^2(t) + \left(\mathrm{H}\{x(t)\}\right)^2} = \sqrt{x^2(t) + \left(x(t) * h(t)\right)^2} \tag{19}$$

$$\varphi(t) = arctg\left(\frac{\mathrm{Im}\, z(t)}{\mathrm{Re}\, z(t)}\right) = arctg\left(\frac{y(t)}{x(t)}\right) = arctg\left(\frac{\mathrm{H}\{x(t)\}}{x(t)}\right) = arctg\left(\frac{x(t) * h(t)}{x(t)}\right) \tag{20}$$

where:

$a(t)$ – a generalized form of the instantaneous amplitude;

$\varphi(t)$ – a generalized form of the instantaneous phase.

Based on these considerations, we can define the following Hilbert transform properties:

- it is carried out in the time domain, this is the same area where the test signal is presented;
- the shape of the imaginary component $y(t)$ of the analytical signal $z(t)$ is uniquely determined by the actual shape of the real component $x(t)$ and vice versa;
- based on the analytical signal $z(t)$ the instantaneous amplitude $a(t)$ and instantaneous phase $\varphi(t)$ can be defined;
- the analytical signal can be called the complex envelop, the knowledge of which allows us to reconstruct easily the signal with the modulated signal. This property is apparent from the pattern (5).

5. DETECTION OF MODULATED SIGNALS, AND DISTORTIONAL SIGNALS

As assumed in this paper low frequency distortion has a significant influence on the modulated signal, describes this relationship (16), as illustrated on Figure 2 and Figure 3 Therefore, it is necessary to remove the disorder of the signal described by formula (15) which is described by formula (16) to obtain a valid modulated signal (14). To do this, we perform the following operations on a received signal:

- the appointment of Hilbert transform and the complex envelope of the received signal $s_n(t)$ is described by formula (16):

$$
\begin{aligned}
&\mathrm{H}\{s_n(t)\} = y(t) = s_n(t) * h(t) = \left(1 + k_{a_n}(t)\cdot n(t)\right)\cdot s(t) * \frac{1}{\pi \cdot t} = \\
&= \frac{1}{\pi}\cdot \int_{-\infty}^{+\infty} \frac{\left(1 + k_{a_n}(\tau)\cdot n(\tau)\right)\cdot s(\tau)}{t-\tau} d\tau = \frac{1}{\pi}\cdot \int_{-\infty}^{+\infty} \frac{s(\tau) + k_{a_n}(\tau)\cdot n(\tau)\cdot s(\tau)}{t-\tau} d\tau = \\
&= \frac{1}{\pi}\cdot \int_{-\infty}^{+\infty} \frac{s(\tau)}{t-\tau} d\tau + \frac{1}{\pi}\cdot \int_{-\infty}^{+\infty} \frac{k_{a_n}(\tau)\cdot n(\tau)\cdot s(\tau)}{t-\tau} d\tau = \frac{U_{c_m}}{\pi}\cdot \int_{-\infty}^{+\infty} \frac{\cos\left(2\cdot\pi\cdot f_c\cdot\tau\right)}{t-\tau} d\tau + \\
&+ \frac{k_a\cdot U_{c_m}\cdot U_{m_m}}{\pi}\cdot \int_{-\infty}^{+\infty} \frac{\cos\left(2\cdot\pi\cdot f_m\cdot\tau\right)\cdot\cos\left(2\cdot\pi\cdot f_c\cdot\tau\right)}{t-\tau} d\tau + \\
&+ \frac{U_{n_m}}{\pi}\cdot \int_{-\infty}^{+\infty} \frac{\cos\left(2\cdot\pi\cdot f_n\cdot\tau\right)\cdot\cos\left(\varphi_n(\tau)\right)\cdot\cos\left(2\cdot\pi\cdot f_c\cdot\tau\right)}{t-\tau} d\tau - \\
&- \frac{U_{n_m}}{\pi}\cdot \int_{-\infty}^{+\infty} \frac{\sin\left(2\cdot\pi\cdot f_n\cdot\tau\right)\cdot\sin\left(\varphi_n(\tau)\right)\cdot\cos\left(2\cdot\pi\cdot f_c\cdot\tau\right)}{t-\tau} d\tau
\end{aligned}
\tag{21}
$$

It can be noted that the Hilbert transform described by (21) is the sum of four Hilbert transformations to be examined individually [3]. In order to determine the pattern we are interested in describing the Hilbert transform distortional received modulated signal. Hilbert transform to the designated individual components contained in the formula (21) will be used instead of as Fourier transform (22) and (23) and the method of projections (24) and (25).

$$
\frac{U_{c_m}}{\pi}\cdot \int_{-\infty}^{+\infty} \frac{\cos\left(2\cdot\pi\cdot f_c\cdot\tau\right)}{t-\tau} d\tau = \frac{U_{c_m}}{\pi}\cdot\sin\left(2\cdot\pi\cdot f_c\cdot t\right) \tag{22}
$$

$$
\begin{aligned}
&\frac{k_a\cdot U_{c_m}\cdot U_{m_m}}{\pi}\cdot \int_{-\infty}^{+\infty} \frac{\cos\left(2\cdot\pi\cdot f_m\cdot\tau\right)\cdot\cos\left(2\cdot\pi\cdot f_c\cdot\tau\right)}{t-\tau} d\tau = \\
&= \frac{k_a\cdot U_{c_m}\cdot U_{m_m}}{\pi}\cdot\sin\left(2\cdot\pi\cdot f_m\cdot t\right)\cdot\sin\left(2\cdot\pi\cdot f_c\cdot t\right)
\end{aligned}
\tag{23}
$$

$$\frac{U_{n_m}}{\pi}\cdot\int_{-\infty}^{+\infty}\frac{\cos(2\cdot\pi\cdot f_n\cdot\tau)\cdot\cos(\varphi_n(\tau))\cdot\cos(2\cdot\pi\cdot f_c\cdot\tau)}{t-\tau}d\tau\approx$$

$$\approx\frac{U_{n_m}}{4\cdot\pi}\cdot\sin\left[2\cdot\pi\cdot\tau\cdot(f_n+f_c)+\varphi_n(\tau)\right]+$$

$$+\frac{U_{n_m}}{4\cdot\pi}\cdot\sin\left[2\cdot\pi\cdot\tau\cdot(f_n+f_c)-\varphi_n(\tau)\right]+ \tag{24}$$

$$+\frac{U_{n_m}}{4\cdot\pi}\cdot\sin\left[2\cdot\pi\cdot\tau\cdot(f_n-f_c)+\varphi_n(\tau)\right]+$$

$$+\frac{U_{n_m}}{4\cdot\pi}\cdot\sin\left[2\cdot\pi\cdot\tau\cdot(f_n-f_c)-\varphi_n(\tau)\right]$$

$$\frac{U_{n_m}}{\pi}\cdot\int_{-\infty}^{+\infty}\frac{\sin(2\cdot\pi\cdot f_n\cdot\tau)\cdot\sin(\varphi_n(\tau))\cdot\cos(2\cdot\pi\cdot f_c\cdot\tau)}{t-\tau}d\tau\approx$$

$$\approx\frac{U_{n_m}}{4\cdot\pi}\cdot\sin\left[2\cdot\pi\cdot\tau\cdot(f_n+f_c)-\varphi_n(\tau)\right]+$$

$$-\frac{U_{n_m}}{4\cdot\pi}\cdot\sin\left[2\cdot\pi\cdot\tau\cdot(f_n+f_c)+\varphi_n(\tau)\right]+ \tag{25}$$

$$+\frac{U_{n_m}}{4\cdot\pi}\cdot\sin\left[2\cdot\pi\cdot\tau\cdot(f_n-f_c)-\varphi_n(\tau)\right]+$$

$$-\frac{U_{n_m}}{4\cdot\pi}\cdot\sin\left[2\cdot\pi\cdot\tau\cdot(f_n-f_c)+\varphi_n(\tau)\right]$$

Correctness of the solutions envisaged (24) and (25) was confirmed in a numerical way. Aggregation of results presented in patterns (22), (23), (24) and (25) can identify the Hilbert transform the received signal on the basis of its complex envelope. Based on the formula:

$$s_n(t)=\mathrm{Re}\left[\underline{s}(t)\cdot z_n(t)\right] \tag{26}$$

where:

$\underline{s}(t)$ – complex carrier signal, which is a modulated signal without distortion;

$z_n(t)=s_n(t)+j\cdot y(t)$ – complex envelope;

$s_n(t)$ – signal received;

you can specify the carrier signal that interests us $s(t)$. The algorithm of proposed method is shown on Figure 4.

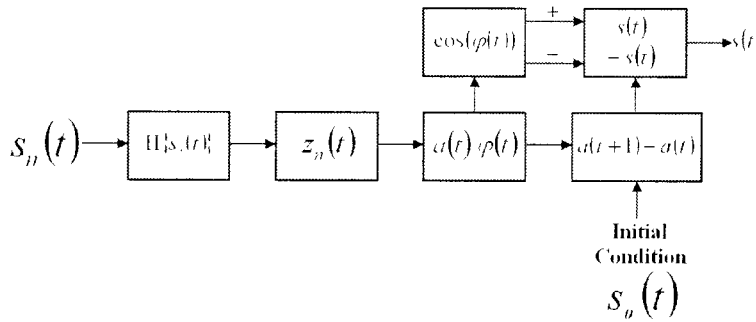

Fig. 4. The algorithm of proposed method

6. CONCLUSIONS

- the proposed method significantly improves the possibility of amplitude modulation, and thereby increases the area of application;
- it is indicated how the analysis of the received signal containing the distortion can easily eliminate them. Thanks to the demodulation we can use simple demodulation systems, for example, a peak detector;
- the correctness of the proposed algorithm shows the results in Table 1.

Table 1. Comparative table of the results of theoretical and obtained based on the proposed method

t [s]	$s(t)$ [V] theoretical values	$\cos(\varphi(t))$ calculated values	$a(t)$ [V] calculated values	$s(t)$ [V] calculated values
0.00000	0.36000	0.99907	0.41657	0.36000
0.00005	–0.35217	–0.99900	0.40825	–0.35168
0.00010	0.32944	0.99883	0.38465	0.32809
0.00015	–0.29405	–0.99854	0.34840	–0.29183
0.00020	0.24944	0.99801	0.30295	0.24638
0.00025	–0.20000	–0.99706	0.25270	–0.19613
0.00030	0.15056	0.99529	0.20250	0.14594
0.00035	–0.10595	–0.99198	0.15723	–0.10067
0.00040	0.07056	0.98614	0.12127	0.06470
0.00045	–0.04783	–0.97817	0.09800	–0.04144
0.00050	0.04000	0.97310	0.08943	0.03286
0.00055	–0.04783	–0.97623	0.09612	–0.03955
0.00060	0.07056	0.98378	0.11743	0.06086
0.00065	–0.10595	–0.99007	0.15138	–0.09481
0.00070	0.15056	0.99388	0.19462	0.13805
0.00075	–0.20000	–0.99599	0.24277	–0.18621
0.00080	0.24944	0.99716	0.29099	0.23443
0.00085	–0.29405	–0.99781	0.33442	–0.27785
0.00090	0.32944	0.99817	0.36866	0.31209
0.00095	–0.35217	–0.99834	0.39025	–0.33369

Table 1 continuous

0.00100	0.36000	0.99837	0.39697	0.34040
0.00105	–0.35217	–0.99826	0.38804	–0.33147
0.00110	0.32944	0.99800	0.36424	0.30767
0.00115	–0.29405	–0.99749	0.32779	–0.27122
0.00120	0.24944	0.99656	0.28219	0.22562
0.00125	–0.20000	–0.99484	0.23181	–0.17525
0.00130	0.15056	0.99146	0.18156	0.12499
0.00135	–0.10595	–0.98462	0.13633	–0.07976
0.00140	0.07056	0.97120	0.10055	0.04400
0.00145	–0.04783	–0.95056	0.07758	–0.02101
0.00150	0.04000	0.93658	0.06911	0.01254
0.00155	–0.04783	–0.94646	0.07539	–0.01883
0.00160	0.07056	0.96705	0.09604	0.03948
0.00165	–0.10595	–0.98183	0.12942	–0.07285
0.00170	0.15056	0.98969	0.17223	0.11566
0.00175	–0.20000	–0.99365	0.22008	–0.16351
0.00180	0.24944	0.99569	0.26805	0.21148
0.00185	–0.29405	–0.99679	0.31127	–0.25471
0.00190	0.32944	0.99737	0.34534	0.28878
0.00195	–0.35217	–0.99766	0.36679	–0.31022
0.00200	0.36000	0.99773	0.37337	0.31680

BIBLIOGRAPHY

[1] Stranneby D., 2004. Cyfrowe przetwarzanie sygnałów. BTC, Warszawa.
[2] Haykin S., 2004. Systemy telekomunikacyjne. WKŁ, Warszawa.
[3] Szabatin J., 2007. Podstawy teorii sygnałów. WKŁ, Warszawa.

METODA ODZYSKIWANIA WŁAŚCIWEJ OBWIEDNI ZESPOLONEJ ZABURZONEGO SYGNAŁU ZMODULOWANEGO AMPLITUDOWO W OPARCIU O PRZEKSZTAŁCENIE HILBERTA

Streszczenie

W pracy przedstawiono definicję przekształcenia Hilberta oraz związane z nim zagadnienia analitycznej reprezentacji sygnału oraz splotu sygnałów. Określono metodę wyznaczania obwiedni sygnałów zmodulowanych amplitudowo z wykorzystaniem przekształcenia Hilberta. Omówiono korzyści wynikające ze stosowania niniejszej metody przy stosowaniu transmisji radiowej, na którą wpływ mają zakłócenia spowodowane sygnałami niskoczęstotliwościowymi, których źródłem może być sieć elektroenergetyczna. Rozpatrywane zagadnienia teoretyczne poparto konkretnymi przykładami.

Słowa kluczowe: przekształcenie Hilberta, sygnał analityczny, sygnał zmodulowany amplitudowo, obwiednia sygnału

Publikacje Wydawnictw Uczelnianych
Uniwersytetu Technologiczno-Przyrodniczego w Bydgoszczy
można nabywać w

Księgarni Wydawnictw Uczelnianych
(Budynek Regionalnego Centrum Innowacyjności)
ul. Prof. S. Kaliskiego 7, 85-789 Bydgoszcz
tel. 52 340 80 53
http://ksiegarnia.utp.edu.pl

ISSN 0209-0570